DOI: 10.1002/cphc.200800691

Tailoring Disorder and Dimensionality: Strategies for Improved Solid Oxide Fuel Cell Electrolytes

Javier Garcia-Barriocanal,[a] Alberto Rivera-Calzada,[a] Maria Varela,[b] Zouhair Sefrioui,[a] Mario R. Díaz-Guillén,[c] Karla J. Moreno,[c] José A. Díaz-Guillén,[c] Enrique Iborra,[d] Antonio F. Fuentes,[c] Stephen J. Pennycook,[b] Carlos Leon,[a] and Jacobo Santamaria*[a]

Reducing the operation temperature of solid oxide fuel cells is a major challenge towards their widespread use for power generation. This has triggered an intense materials research effort involving the search for novel electrolytes with higher ionic conductivity near room temperature. Two main directions are being currently followed: the use of doping strategies for the synthesis of new bulk materials and the implementation of nanotechnology routes for the fabrication of artificial nanostructures with improved properties. In this paper, we review our recent work on solid oxide fuel cell electrolyte materials in these two directions, with special emphasis on the importance of disorder and reduced dimensionality in determining ion conductivity. Substitution of Ti for Zr in the $A_2Zr_{2-y}Ti_yO_7$ (A = Y, Dy, and Gd) series, directly related to yttria stabilized zirconia (a common fuel cell electrolyte), allows controlling ion mobility over wide ranges. In the second scenario we describe the strong enhancement of the conductivity occurring at the interfaces of superlattices made by alternating strontium titanate and yttria stabilized zirconia ultrathin films. We conclude that cooperative effects in oxygen dynamics play a primary role in determining ion mobility of bulk and artificially nanolayered materials and should be considered in the design of new electrolytes with enhanced conductivity.

1. Introduction

Fuel cells are electrochemical devices to generate energy out of hydrogen. The principle of operation was discovered by the British physicist William Robert Grove who in 1839 successfully reversed the electrolysis process.[1] In the same way that water molecules are split into their constituent oxygen and hydrogen by the passage of an electric current, in a fuel cell, oxygen and hydrogen are combined to produce electricity and water. The essential constituents are two conducting electrodes which capture hydrogen and oxygen independently, separated by an electrolyte which is permeable to ions (either hydrogen or oxygen depending on the fuel cell category) but not to electrons. An electrode catalytic process yields the ionic species which are transported through the electrolyte while electrons blocked by the electrolyte stream through the external circuit. The electric current flows as long as hydrogen and oxygen are being supplied to maintain the electrode processes, and the device behaves as a battery with the capability of being refuelled. Hydrogen is a green carrier of energy and water is a green carrier of hydrogen. Hydrogen is created from water injecting energy at the point of production and energy is returned when hydrogen is oxidized at the point of use; this configuration represents a sustainable hydrogen-water cycle. Despite the appealing potential for a "hydrogen economy", the pathway is still fraught with problems.[2]

Current fuel-cell technology allows the use of alcohol or hydrocarbon fuels, although this requires a fuel processing stage which reduces efficiency and increases costs. Moreover, CO byproducts of the reformation of hydrocarbon fuels reduce the activity of catalysts and limit efficiency of the devices. Thus important materials selection and manufacturing problems derived from the particular fuel and temperature of operation have limited, so far, the fuel cells share of the electrical power market. Polymeric membrane (PEMFC)- or phosphoric acid fuel cells (PAFC) operating at low temperatures are the preferred option for transportation, due to their quite large efficiencies (50%) compared with gasoline combustion engines (25%). Other uses such as battery replacements for personal electronics, stationary or portable emergency power are also being considered. There are, however, severe cost drawbacks related to the use of Pt catalysts which are scarce and expensive. Solid oxide fuel cells (SOFC) operating at high temperatures are a better option for stationary power generation due to their scalability. Here O^{2-} ions are the mobile species which travel at

[a] Dr. J. Garcia-Barriocanal, Dr. A. Rivera-Calzada, Prof. Z. Sefrioui, Prof. C. Leon, Prof. J. Santamaria
GFMC, Universidad Complutense de Madrid
Madrid 28040 (Spain)
Fax: (+34) 913945196
E-mail: jacsan@fis.ucm.es

[b] Dr. M. Varela, Dr. S. J. Pennycook
Materials Science & Technology Division
Oak Ridge National Laboratory, Oak Ridge, TN 37831 (USA)

[c] M. R. Díaz-Guillén, Dr. K. J. Moreno, J. A. Díaz-Guillén, Dr. A. F. Fuentes[+]
Cinvestav-Saltillo, Ap. Postal 663
25000 Saltillo, Coahuila (Mexico)

[d] Prof. E. Iborra
Escuela Técnica Superior de Ingenieros de Telecomunicaciones
Universidad Politécnica de Madrid, Madrid 28040 (Spain)

[+] Current address:
ARAID-Instituto de Ciencia de Materiales de Aragon
C.S.I.C.-Universidad de Zaragoza, 50009 Zaragoza (Spain)

 © 2009 Wiley-VCH Verlag GmbH & Co. KGaA, Weinheim

elevated temperatures (800–1000 °C) through a solid electrolyte material to react with H^+ ions in the anode to produce water. The high operation temperatures favour internal fuel reformation, electrode processes and ionic migration through the electrolyte, but impose serious restrictions on materials selection due to thermal stress or fatigue. Using lower temperatures gives rise to ohmic losses related to the lower ionic conductivity of the electrolyte, which seriously limit the performance of the devices.

The electrolyte is the "heart of the SOFC" and there is general agreement that substantial effort should be made to optimize its properties. In particular, reducing the operating temperature of solid oxide fuel cells without compromising the electrode kinetics and the internal resistance of the cell, is a major materials research goal involving the search for novel electrolytes, although it may also impact active catalysts for electrode processes (oxygen reduction and hydrogen oxidation) and suitable ionic and electronic conductivities compatible with the electrolyte. There are currently two main strategies in the search of novel materials for reduced temperature fuel cell operation: one is synthesizing new bulk materials with larger conductivity values and the other is the use of nanotechnology routes to arrive at artificial nanostructures with improved properties.

The search for novel materials has allowed reduction of the operating temperature to the range of 500–750 °C in a category of fuel cells called intermediate temperature (IT) fuel cells. Operation at lower temperature has stimulated a strong effort in the search for novel electrolytes and also for electrode materials.[3–8] Regarding the electrolyte, the figure of merit of 0.15 $\Omega\,cm^2$ for the area specific resistance (ASR, resistivity × thickness) for practical fuel cell application requires increasing the bulk conductivity above 0.01 $S\,cm^{-1}$ (the lower limit for 15 microns thick electrolytes). While this limit is reached at 950 °C for yttria stabilized zirconia (YSZ) electrolytes, it has been achieved in the 500 °C range using $Ce_{1-x}M_xO_{2-\delta}$ (M: Sm, Gd, Ca, Mn) or doped $LaGaO_3$ compounds.[9] A commonly used strategy to increase the conductivity of the electrolyte is to chemically substitute elements that preferentially increase the concentration of the mobile specie. Unfortunately, there is often an optimum level of doping beyond which the conductivity begins to decrease. At the optimal level, the only way to increase conductivity further is to raise the operating temperature to enhance the mobility of the defects.[10] Among oxide-ion conductors, those of anion-deficient fluorite structure like yttria stabilized zirconia (YSZ) , $x\ Y_2O_3$: $(1-x)\ ZrO_2$, are extensively used today as electrolytes in SOFCs.[9,10] Doping with Y_2O_3 is known to stabilize the cubic fluorite structure of ZrO_2 and to supply the oxygen vacancies responsible for the ionic conduction.[11] These materials are characterized by a large number of mobile oxygen vacancies, which are randomly distributed in the structure and thus give rise to a completely disordered anion (oxygen) sublattice. Related to these materials, those with the pyrochlore structure, such as $A_2Zr_2O_7$ (A: Y, Dy, Gd) have also received significant attention in recent years mainly due to their structural flexibility and high compositional diversity, some of them showing also a high oxide-ion conductivity.[12–14] The pyrochlore cubic crystal structure (S.G. 227) can be derived from that of a fluorite by doubling the unit cell, removing one out of eight anions, and placing cations and anions in four crystallographically nonequivalent sites. An important feature of these materials is that they present a different degree of cation and anion disorder, depending on the composition and on the synthesis procedure, varying from an almost *ideal* (ordered) pyrochlore structure to a (completely disordered) fluorite structure.[15,16] Different degrees of structural disorder can be obtained in systems of solid solutions by using the appropriate substitutions on the A and B sites of the pyrochlore structure,[17] thus allowing carrier density and mobility to be changed over wide ranges.

On the other hand ionic transport is known to be strongly modified in nanomaterials,[18–20] and thus, nanotechnology is expected to have a large impact on the next generation of fuel cells, particularly in the areas of catalysts, membranes and hydrogen storage,[21,22] although its use in SOFC has to be undertaken with care due to possible microstructural changes at the high operational temperatures.[23] The term nanoionics has been coined to embrace the new concepts in ion transport and electrochemical storage which result from confinement in nanostructures.[24] Space charge effects are an interesting family of nanoionic size effects which show up when sample dimensions are comparable to the extension of the space charge region (or Debye length).[25–27] It is well known that the energy for defect generation may be different at surfaces or boundaries. In ionic compounds, the accumulation of defects breaks charge neutrality and creates an electric field which is screened over the Debye length by depletion or accumulation of mobile charges.[28] The Debye length is thus the scale for charge inhomogeneities, over which changes in the density of mobile carriers can be expected. Quite remarkable is the large enhancement of the electronic conductivity in the mixed ionic-electronic conductor CeO_2 occurring at grain boundaries due to accumulation of vacancies at the grain boundary cores.[29] Electrons accumulate to screen the resulting electric field, giving rise to an increase of the electronic conductivity which becomes dominant when grain size is reduced down to the 10 nm scale. The occurrence of space charge effects in YSZ has been a subject of controversy in recent years. While some authors have reported increases of the ionic conductivity in nanogranular samples,[30] others have found no changes[31] or even decreases[32,33] of the conductivity of samples produced with different synthesis routes and with different grain sizes and dopant concentrations. ^{18}O tracer diffusion experiments assisted by secondary ion mass spectroscopy also yield contradictory results: while 3 orders of magnitude increase of the diffusion coefficient as compared with bulk samples has been reported in nanocrystalline thin films,[34] bulk nanocrystalline ceramics show no change.[35] The explanation of the increases in terms of space charge effects is also not straightforward in this case, since very small values of the Debye screening length of the order of 0.1 nm result for typical dopant concentrations (8% YSZ) at intermediate temperatures (500 °C). Clearly further work is necessary to clarify this issue,[36] but the possibility of an enhanced ionic conductivity in nanostructures has triggered

 © 2009 Wiley-VCH Verlag GmbH & Co. KGaA, Weinheim

large activity in the field, due to its possible impact in electrolytes with lower operation temperatures or in electrodes with higher rates. Moreover, size effects may be relevant for the electrode reaction itself giving rise to increased reactivity as shown for nanocrystalline ceria electrodes where nanostructuring promotes the charge transfer reaction at the electrode–electrolyte interface.[37] Nanostructured samples may also help in improving catalysts. Pt is an expensive and scarce material for use in low temperature fuel cells. Using nanoparticles[38,39] or substituting Pt by a second element leaving the surface layer intact to break O–O bonds with the same efficiency[40,41] are strategies to reduce the amount of Pt used while still achieving the required catalytic activity.

Another interesting new direction in nanoionics consists of making use of thin film technology to design "artificial materials" with tailored structure to optimize fuel-cell materials. Thin film growth techniques allow the combined growth of thin layers of different materials in heterostructures with a high crystalline perfection and very controlled properties. These heterostructures have played a decisive role in recent electronic and communication technology, for example in semiconductor quantum wells and superlattices,[42] or in metallic superlattices[43] with giant magnetoresistance[44] which is of paramount importance in information storage. Thin-film heterostructures are also important in the development of future electrochemical devices for energy generation and storage. The large changes in the ionic conductivity found in thin-film structures have stimulated great interest in these kinds of samples as to define an important direction in the field of nanoionics. Space charge effects may give rise to large changes in the ionic conductivity at surfaces or interfaces over length scales of the order of the Debye screening length. The discontinuity of the free energy at interfaces naturally results in charge-transfer processes which break charge neutrality and may profoundly change the carrier density. Recently, Maier and colleagues[45] have shown dramatic increases of the ionic conductivity in layered thin-film superlattices alternating Ba and Ca fluorides, and interpreted it as the result of the transfer of fluorine ions into the CaF_2 side. This yields enhanced vacancy concentration in the Ba side when the thickness of the individual layers become comparable to the size of the space charge region.

Several studies have reported modified ionic conductivity in thin films involving YSZ, although as in the case of bulk samples there are conflicting experimental evidences and contradictory interpretations. Tuller and co-workers[46] have found an increase of the ionic conductivity of thin films of YSZ deposited by spin coating on Al_2O_3, when their thickness is reduced to the 10 nm range. The magnitude of the increase is between one and two orders of magnitude (in the temperature range 550–900 °C) and is accompanied by a reduction of the activation energy from 1.15 to 0.93 eV. More recently, Kosacki et al.[47] reported a strong increase of the conductivity of 10% Y_2O_3 doped YSZ epitaxial thin films grown on MgO when thickness is reduced down to 15 nm. The conductivity increase by more than two orders of magnitude at 400 °C is accompanied by a reduction of the activation energy down to 0.62 eV. Authors attribute the conductivity increase to a highly conducting 1 nm layer at the YSZ/MgO interface. A moderate conductivity increase (slightly above one order of magnitude) was found by Karthikeyan et al.[48] for 17 nm YSZ polycrystalline multiphase samples grown on MgO. On the other hand Guo et al.[49] found a decrease of the ionic conductivity of 12 nm thick nanograined polycrystalline YSZ thin films deposited on MgO as compared to 8% Y_2O_3 doped bulk ceramics and essentially no change of the activation energy. The possibility of increasing electrolyte conductivity by the use of thin film structures is a very encouraging route to optimize fuel-cell materials. However, the controversial results, which are similar to those found in bulk nanogranular materials, clearly outline the need of further studies.

Herein, we review our recent work on solid oxide fuel cell electrolyte materials, we report on our activity on the two mentioned directions: chemical substitutions for improved bulk materials and artificially nanolayered materials with optimized interface properties. Specifically, in the first scenario, we examine the effect of ion- ion correlations on the long range ion mobility of oxygen conductors derived from YSZ. Long-range migration of oxygen ions takes place by thermally activated hopping to adjacent oxygen vacancies, which yields a dc conductivity of the form $\sigma_{dc} = (\sigma_\infty/T)\exp(-E_{dc}/kT)$. Increasing conductivity would therefore require increasing the prefactor σ_∞ and/or decreasing the activation energy E_{dc}. However, increasing the number of charge carriers to increase σ_∞ leads to an undesired increase in E_{dc} and eventually to lower conductivity values,[10] thus limiting the strategies to obtain high oxygen conductivity at lower temperatures. The origin of this behavior has remained not well understood.[9,10,50,51] We show that the increase of the activation energy E_{dc} is controlled by cooperative effects in oxygen dynamics, which play a primary role in determining ionic conductivity values.[52–57] In the second scenario we have explored the use of interface effects in artificially layered materials to arrive at highly ion-conducting superlattices. We will describe the strong enhancement of the conductivity occurring at the interfaces of superlattices made by alternating strontium titanate and yttria stabilized zirconia.[58] In these layered nanostructures a substantial fraction of the atoms are close to the interfaces, where the density of mobile species (vacancies) and mobility may be enhanced as compared to bulk values due to space-charge effects. Epitaxial strain is also an important factor to consider since a distorted interface structure may be also responsible for modified ion diffusivity.

2. Ionic Conductivity and Ion–Ion Correlations in Bulk Oxygen Conducting Electrolytes

Materials of composition $A_2Zr_{2-y}Ti_yO_7$ (A = Y, Dy, and Gd) are directly related to YSZ with 33% mol yttria content, $Y_2Zr_2O_7$ (0.33 Y_2O_3: 0.67 ZrO_2). They show a high oxide ion conductivity, even comparable to that of YSZ with 8–10% mol yttria content which is currently used as electrolyte in SOFCs.[59] It is well known[16,60] that oxygen diffusion in these materials takes place by vacancy hopping from 48*f* to 48*f* sites, and while the oxygen occupancy of 48*f* sites is 1 (or close to 1) in a highly

 © 2009 Wiley-VCH Verlag GmbH & Co. KGaA, Weinheim

ordered pyrochlore structure, it decreases progressively as cation disorder increases towards the anion-deficient fluorite structure. For example, the cation and anion substructures in the $A_2Zr_{2-y}Ti_yO_7$ solid solution disorder gradually as the Zr content increases, leading to the appearance of oxygen vacancies at 48*f* sites. Besides this chemically induced disorder (Zr substitution by Ti), we have previously shown[57] that it is also possible to induce different degrees of structural ordering in the oxygen sublattice by different thermal annealing treatments of highly disordered pyrochlores as obtained by a mechanical milling synthesis. Thus, interestingly, the number of mobile oxygen vacancies increases significantly (by about two orders of magnitude) as structural disorder increases in these pyrochlores, providing an appealing scenario to study the influence of ion–ion interactions on the long range ion transport and dc conductivity values.

Information about ion dynamics can be obtained from impedance spectroscopy measurements.[61] At high frequencies and low temperatures isothermal ac conductivity data curves show a Jonscher-type[62] power law dependence of the form $\sigma'(\omega) \propto \omega^n$ with a fractional exponent *n*, and increasing temperature and/or decreasing frequency leads to a regime with a frequency independent conductivity "plateau", σ_{dc}, which is the bulk dc conductivity (see Figure 1 a). As observed in the inset to Figure 1 a it is found that the dc conductivity shows a thermally activated behavior with an activation energy E_{dc}. An alternative representation of experimental conductivity data can be made by plotting the frequency dependence of the complex electric modulus, $M^*(\omega)$, [see Figure 1 b] which is directly related to the complex conductivity as $M^*(\omega) = 1/\varepsilon^*(\omega) = j\omega\varepsilon_0/\sigma^*(\omega)$, with ε_0 the permittivity of vacuum. The use of the electric modulus allows one to obtain the relaxation function in the time domain, $\Phi(t)$, for the decay of the electric field inside the material under the constraint of a constant displacement vector.[61,63] The frequency dependence of the electric modulus is given directly by the Laplace transform of the time derivative of the relaxation function, as shown in Equation (1)

$$M^*(\omega) = \frac{1}{\varepsilon_\infty}\left[1 - \int_0^\infty \left(-\frac{d\Phi}{dt}\right) e^{-j\omega t} dt\right] \quad (1)$$

where ε_∞ is the permittivity value at high frequencies. The relaxation function $\Phi(t)$ in ionic conductors is usually found to be non-exponential and can be well described by Kohlrausch–Williams–Watts (KWW) functions[63,64] of the form of Equation (2):

$$\Phi(t) = \exp(-(t/\tau)^{1-n}), \;\; 0 < (1-n) \leq 1 \quad (2)$$

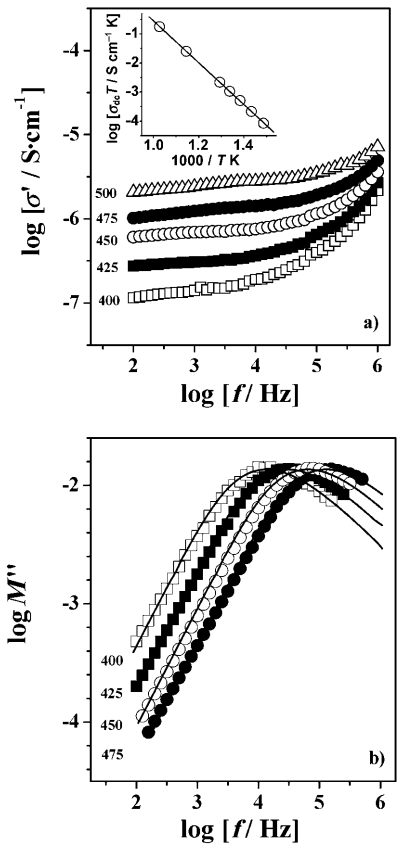

Figure 1. a) Frequency dependence of the electrical conductivity, $\sigma'(\omega)$, at different temperatures between 400 and 500 °C, for $Y_2Zr_2O_7$ as a representative composition. The inset shows the thermally activated behavior of the dc conductivity. b) Imaginary part of the electric modulus for selected data sets of (a) (corresponding to temperatures 400, 425, 450 and 475 °C).

The relaxation time τ is a characteristic time for the ion-hopping process and it is therefore thermally activated with the same activation energy as the *dc* conductivity. The exponent *n* in the KWW function gives rise to the power law frequency dependence of the ac conductivity at the highest frequencies. Solid lines in Figure 1 b are best fits to KWW functions, from which the exponent *n* can be determined. Different models have been proposed to analyze electrical relaxation data in ionic conductors,[65,66] where the fractional exponent *n* that characterizes ion hopping dynamics is related to the existence of cooperative effects among mobile ions, that is, in the absence of interactions among mobile ions (independent random ion hopping), the exponent *n* would be 0, while *n* would tend to 1 for a completely correlated ion motion.[67,68] In particular, according to Ngai's coupling model,[66] the exponent *n* and the dc activation energy E_{dc} are related through the important relation given in Equation (3)

$$E_{dc} = E_a/(1-n) \quad (3)$$

where the energy E_a is the actual barrier that mobile ions must overcome to hop to neighboring sites and the difference $E_{dc} - E_a = nE_{dc}$ accounts for the energy penalty that ion–ion interactions impose to long range ion transport or dc conductivity. Thus, for a given energy barrier E_a, enhanced ion–ion interaction leads to a higher degree of cooperative motion in the ion-hopping process, which corresponds to a higher value of *n* and consequently a higher activation energy E_{dc} for long-range ionic transport.

Increasing carrier density will generally strengthen also the ion–ion interaction, thus increased carrier concentration may not be enough to achieve increased conductivity. Carrier con-

 © 2009 Wiley-VCH Verlag GmbH & Co. KGaA, Weinheim

centration can be controlled over a wide range in the $A_2Zr_{2-y}Ti_yO_7$ (A = Y, Dy, and Gd) system by changing the Zr content as the result of induced disorder. Specifically, increasing the Zr content increases cation disorder in the pyrochlore structure and the number of mobile oxygen vacancies, and enhanced ion–ion interactions are thus expected. Figure 2 shows the values obtained from impedance spectroscopy measurements for the exponent n, the dc activation energy E_{dc}, and the calculated energy barrier E_a by using Equation (3), for different $A_2Zr_{2-y}Ti_yO_7$ (A = Y, Dy, and Gd) compositions. Experimental data clearly illustrate that there is a systematic increase in both n and E_{dc} when increasing the Zr content in the B sites for a given cation in the A sites, while the energy barrier E_a remains constant within experimental error. Thus, as expected, increased carrier concentration may result in a decrease of the conductivity.

We have also shown that the degree of disorder for a given composition can be modified without doping or changing the cations. Mechanical milling allows the preparation of partially disordered $A_2Zr_{2-y}Ti_yO_7$ pyrochlores,[69] where the structural disorder has been found to be systematically relieved by annealing. By increasing the annealing temperature a more ordered structure is obtained, as determined from Raman spectroscopy and X-ray diffraction.[55] Again a decrease of E_{dc} and a concomitant decrease of the exponent n is observed when increasing structural order (increasing annealing temperature).

Another interesting possibility is modifying the single ion activation energy, E_a, without changing correlations. This finding is illustrated in Figure 3 showing the systematic decrease of both E_a and E_{dc} activation energies when increasing the cation size in the A sites in highly disordered pyrochlore-type ionic conductors. All compositions in Figure 3 are pure zirconates and it is the cation in the A sites which is fully or partially substituted. They all present a similar degree of structural disorder, as indicated by the large and similar value of the exponent n. In this case, the lower activation energies found when increasing the cation size in the A sites would directly arise from a more open structure in a larger unit cell.[57]

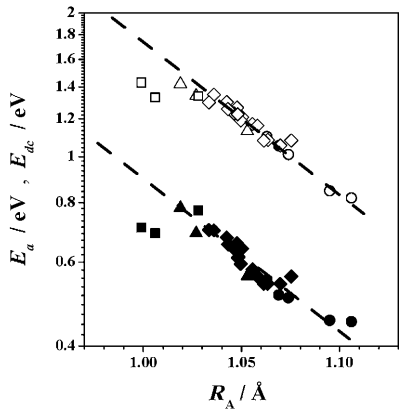

Figure 3. Single ion and long range activation energies, E_a (solid symbols) and E_{dc} (open symbols) as a function of the cation size in the A sites in highly disordered pyrochlore ionic conductors of composition $A_2Zr_2O_7$, $A_{1.7}Mg_{0.3}Zr_2O_7$ (A = Y, Dy and Gd), and $Gd_{2-y}Ln_yZr_2O_7$ (Ln = Er, Y, Dy, Sm, Nd, La, $0 \leq y \leq 1$).

3. Ionic Conductivity and Interface Phenomena in Complex Oxide Superlattices

The enhanced conductivity reported by Kosacki et al.[47] in highly textured thin films of YSZ grown on MgO with thickness between 60 and 15 nm, reaching 0.6 $S\,cm^{-1}$ at 800 °C, has been interpreted in terms of a highly conducting interface layer. Furthermore, Azad et al.[70,71] have grown multilayers alternating GDC (gadolinia doped ceria) and ZrO_2 and found a conductivity increase triggered by disorder associated to structure misfit at the interfaces. More recently Peters et al.[72] found that heteroespitaxial CSZ (calcia stabilized zirconia)/Al_2O_3 incoherent superlattices show a strong conductivity increase by more than 60 times as compared to bulk CSZ. They propose that misfit dislocations at the interface promote ion diffusion. In a later work by the same group Korte et al.[73] show that YSZ/Y_2O_3 semicoherent interfaces with somewhat smaller strain 3% show a more modest conductivity increase which is also discussed in terms of the beneficial effect of the interface stress field for ion diffusion. There is in summary a number of recent reports suggesting that interfaces involving YSZ may ex-

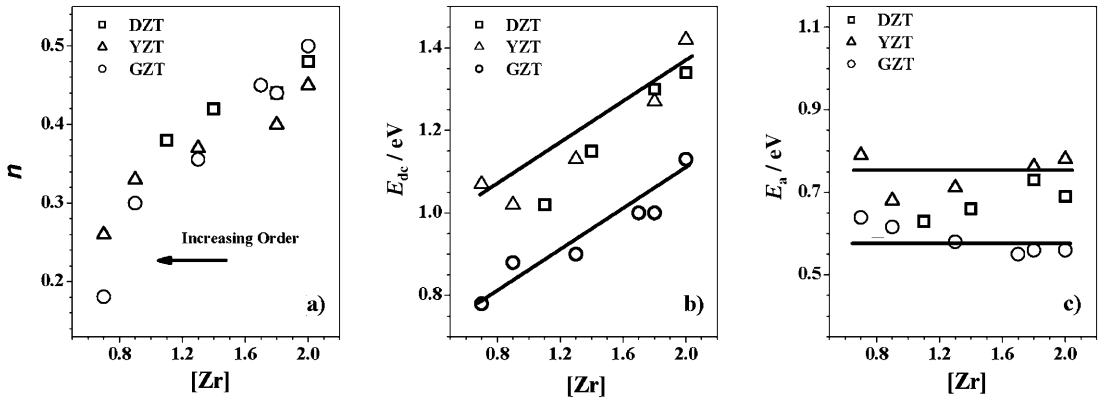

Figure 2. Exponent n (a), the dc activation energy E_{dc} (b), from impedance spectroscopy measurements and the calculated energy barrier E_a (c) by using Equation (3), for different $A_2Zr_{2-y}Ti_yO_7$ (A = Y, Dy, and Gd) compositions.

 © 2009 Wiley-VCH Verlag GmbH & Co. KGaA, Weinheim

hibit enhanced conductivity. Recent advances in the growth of complex oxides have yielded heterostructures with controlled thickness down to the unit cell level (0.3–1 nm). The reduction of one of the dimensions down to the nanometric or subnanometric range opens the way to novel nanoscience phenomena and in the same way that exciting new electronic states have been discovered in complex oxide heterostructures,[74–79] ionic transport is also deeply modified. To explore how interfaces may modify ionic transport in highly coherent (but strained) interfaces, we have grown heterostructures alternating YSZ layers (with 8 mol% nominal yttria content), with insulating $SrTiO_3$ (STO) 10 nm thick layers using a pure oxygen rf sputtering technique. This deposition method combines high temperature (900 °C) with high pressure (3 mbar) to yield a slow and highly thermalized growth resulting in good epitaxial properties.[80–84] Two kinds of samples were grown, STO/YSZ/STO trilayers and superlattices alternating 10 nm thick STO films with YSZ layers with thickness between 62 nm and 1 nm.[58] X-ray diffraction experiments confirm that the ultra thin layer of YSZ grows rotated by 45° around the *c* axis and strained to match the STO lattice (see Figure 4a). Since the bulk lattice constants of STO and YSZ are 0.3905 and 0.514 nm respectively, the epitaxial growth of the YSZ on top of the STO ensures a large expansive strain in the thin YSZ layers of 7% in the *ab* plane. Scanning transmission electron microscopy (STEM) observations have shown that the layers are continuous and flat over lateral distances of a few microns.[58] Figure 4b displays a high resolution annular dark field (or Z-contrast) image of a $[YSZ_{1nm}/STO_{10nm}]_9$ superlattice (with 9 repeats), showing the coherent growth and atomically flat interfaces.[58]

Conductivity was measured using an alternating current, ac, impedance spectroscopy method (see Figure 5). As described for the bulk samples, ac ionic conductivity is customarily described with the phenomenological Jonscher's power law dependence at high frequencies or low temperatures, and a regime with a frequency independent conductivity value, σ_{dc}, when increasing temperature or decreasing frequency.[62] Conductivity power laws are ascribed to non random ion hopping and the exponent *n* measures the degree of correlation between moving species. Figure 5 gathers a set of dispersive conductivity isotherms corresponding to a trilayer with 2 unit cells thick (1 nm) YSZ. A clearly distinct conductivity plateau can be identified, corresponding to the bulk conductivity, σ_{dc}. The conductivity drop towards low frequencies can be ascribed to carriers being blocked at grain boundaries and/or electrodes. For comparison we have also included conductivity data of a YSZ single crystal[85] and of a (thick) 700 nm YSZ thin film grown on (100) MgO covered by a 20 nm gold layer measured in the parallel plate geometry.[86] An Arrhenius plot showing the temperature dependence of the long range conductivity, σ_{dc}, for the YSZ single crystal, the 700 nm thin film, and the 1 nm thick YSZ trilayer, is presented in Figure 5d. A noticeable increase of the conductivity is found in the ultrathin layers as compared to the thick films or bulk samples, which can be as large as eight orders of magnitude close to room temperature. Note that this conductivity increase results both from an increase of the conductivity pre-exponential factor and from a decrease of

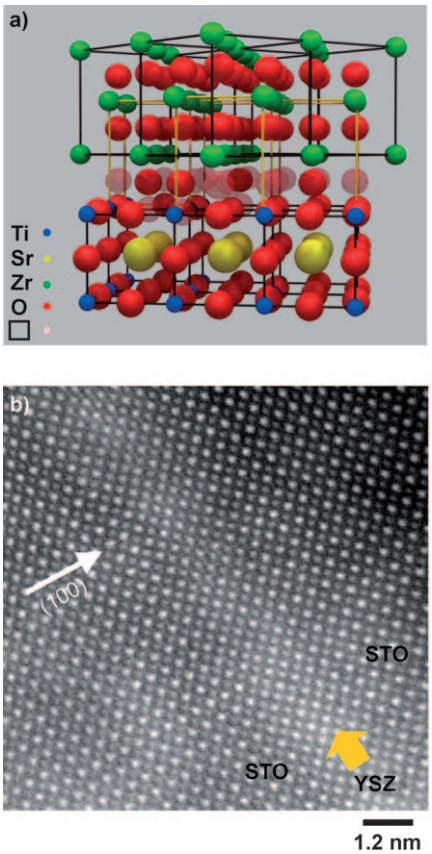

Figure 4. a) Solid spheres model of the YSZ/STO interface showing a 3D view of the interface illustrating the compatibility of the perovskite and fluorite (rotated) structures. Ionic radii are not to scale to better visualize the plane of oxygen vacancies introduced in the interface. Note that the square symbol in the legend represents the empty positions available for oxygen ions at the interface. b) Z-contrast STEM image of the STO/YSZ interface of the $[YSZ_{1\,nm}/STO_{10\,nm}]_9$ superlattice (with 9 repeats), obtained in the VG Microscopes HB603U microscope. A yellow arrow marks the position of the YSZ layer.

the activation energy from values of about 1 eV for bulk samples to 0.6 eV for the ultrathin trilayers. Interestingly, conductivity decreases as the inverse of the YSZ layer thickness when YSZ thickness is increased from 1 up to 30 nm, but the conductance is essentially thickness independent indicating that it is an interface phenomenon. To further test this scenario we have grown superlattices repeating the $[YSZ_{1\,nm}/STO_{10\,nm}]$ growth unit. We have found that conductance scales with the number of interfaces up to a number of 8 (4 bilayer repetitions).[58]

The frequency dispersive conductivity at high frequencies provides further insight into the nature of the high conductivity interface in the YSZ/STO heterostructures. The dispersive conductivity data of Figures 5b and c show that both for single crystals and for thick YSZ layers the power law frequency term with $n \approx 0.55$ is found to dominate over a wide frequency–temperature range. At low temperatures and high frequencies data merge into the weakly temperature dependent near constant loss (NCL) regime characterized by a linear frequency dependence of the ac conductivity. This NCL regime is

 © 2009 Wiley-VCH Verlag GmbH & Co. KGaA, Weinheim

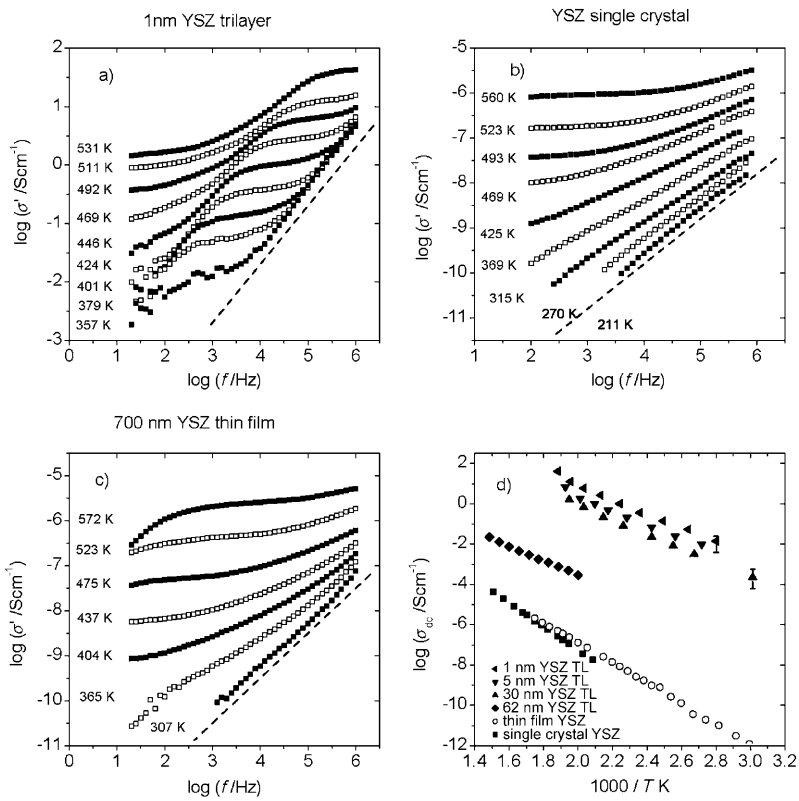

Figure 5. Real part of the conductivity as a function of frequency at several temperatures for a 1 nm YSZ (~8% mol yttria content) trilayer with 10 nm STO top and bottom layers grown on a (100) STO substrate (a), a YSZ single crystal (9.5% mol yttria content) and a 700 nm YSZ film grown on MgO (~8% mol yttria content), (b) and (c). (d) dc conductivity (obtained from the plateaus of σ' plots) as a function of the reciprocal temperature for YSZ single crystal (black squares) and YSZ 700 nm film (open circles). Solid diamonds correspond to a 62 nm thick YSZ trilayer and the triangles showing the colossal enhancement of the conductivity correspond to 30, 5 and 1 nm thick YSZ trilayers (from the bottom to the top).

a ubiquitous term in the ac conductivity of ionic conducting materials which has been ascribed to caged dynamics of the mobile ions at short times (high frequencies).[87–95] The ultrathin YSZ based superlattices, on the other hand, show a very different behavior. The power law conductivity is absent, that is, $n \approx 0$, as shown by the dc plateau directly merging into a NCL term (see Figure 5a). As discussed in the previous paragraphs, the exponent n provides a measure of the penalty introduced by ion–ion correlations in the activation energy for ion diffusion. According to Ngai's coupling model,[66] Equation (3) can be used to quantify the energy barrier for single ion hopping E_a in terms of the exponent n and the long range activation energy for ion transport, E_{dc}. In view of the activation energy E_{dc} of about 1 eV found from the temperature dependence of the long range conductivity σ_{dc} for bulk samples, a value of $E_a = 0.45$ eV results in good agreement with the value reported earlier for single crystals and very close to the 0.49 eV association energy of oxygen vacancies.[96,97] The absence of the fractional power law regime in the trilayer samples is a striking result indicating an uncorrelated ion motion (n close to 0). Thus according to the expression $E_a = (1-n)E_{dc}$, the reduced values of the long range activation energy $E_{dc} = 0.6$ eV found for these samples suggest that the weak ion–ion correlations impose little penalty for long range diffusion which occur essentially at the cost of the single ion activation energy. Uncorrelated ion motion has been only observed in systems with carrier concentration low enough that mobile carriers do not "see" each other.[98] Such a scenario can be excluded in our samples where the large conductivity values in fact indicate a high charge density. This uncorrelated ion diffusion process suggests a sort of interfacial "ionic liquid" probably resulting from the large in-plane expansive strain on the YSZ interface plane, together with the high concentration of vacant oxygen positions and probable positional disorder.

The large conductivity pre-exponential factor of the trilayer samples, 10^7 $(\Omega\,\mathrm{cm})^{-1}$, which are about 2 orders of magnitude larger than in the single crystal samples ($>10^4$ $(\Omega\,\mathrm{cm})^{-1}$), may be discussed in view of the widely accepted expression for the conductivity pre-exponential factor, given in Equation (4)

$$\sigma_\infty = \frac{4\alpha e^2 a^2 \nu_0 N e^{S/k_B}}{k_B} \qquad (4)$$

where α is a geometrical factor, a is the jump distance, ν_0 is the attempt frequency, N is the concentration of oxygen vacancies, S is a configurational entropy term, e is the electron charge and k_B is Boltzmann's constant. The difference could be justified in terms of either an increase in the concentration of oxygen vacancies (N), or of a larger entropy term [$\exp(S/k_B)$] due to an increased number of available positions for the oxygen ions (enhanced positional disorder for the oxygen vacancies). Most likely a combination of both factors is at play. It is quite remarkable that an increase of the disorder in the cation sublattice may actually yield an increase in the ion mobility, what actually constitutes one of the very few cases where the disorder occurring at the interfaces of thin film epitaxial structures yields an improvement of the system properties, instead of a deterioration observed in most practical examples. Moreover, the values of the pre-exponential factor of about 10^7 $(\Omega\,\mathrm{cm})^{-1}$ are comparable to those found in other ion conductors such as β-AgI which shows a value of the pre-exponential factor of 10^8 $(\Omega\,\mathrm{cm})^{-1}$.[99]

The large enhancement of the ionic conductivity found at YSZ/STO interfaces reaches values that enable practical application of the material in SOFC slightly above room tempera-

 © 2009 Wiley-VCH Verlag GmbH & Co. KGaA, Weinheim

ture. This result may have a special impact on single chamber fuel cells where both electrodes are located on the same side of a thin electrolyte deposited onto a substrate,[100] and thus the ionic conductivity flows in a lateral direction parallel to the substrate. The basic ingredients of the conductivity enhancement of the YSZ ultrathin layers are 1) increased number of oxygen vacancies and 2) disorder in the cationic sublattice, which both yield the high pre-exponential factors, and 3) weakly correlated (or uncorrelated) ion motion which provide the low values of the long range activation energy. Most likely these three factors are mutually dependent somehow: it is clear that the increased number of vacancies at the interface may account for the increase in the configurational entropy, however it is not clear how these factors affect the correlation strength individually. According to the experience gathered from the chemical substitution of dopants in bulk samples, disorder seems to act in the direction of strengthening correlations, as well as increased number of carriers, which would promote correlations among them. However, one should not draw far-reaching conclusions from the comparison between the two scenarios of interfaces and chemical substitutions, as they may be fundamentally different in nature.

4. Summary and Outlook

The optimization of electrolytes for low temperature operation of solid oxide fuel cells requires increasing oxide ion conductivity to achieve the required value of 0.01 $S\,cm^{-1}$ closer to room temperature. Ideally this could be accomplished by a simultaneous increase of the density of charge carriers and their mobility (larger configurational entropy and lower activation energy for long range ion motion). Unfortunately, increasing carrier concentration leads to enhanced ion–ion correlations, which introduces an additional energy penalty to the diffusion process that is, larger values of the long range activation energy. Cooperative oxygen ion dynamics is thus a key factor in determining ionic conductivity values, and should be considered in the design of novel conductors with optimized properties. On the other hand, interfaces of heterostructures with nanometer thick layers can be tailored to display large values of ionic conductivity. The reduced dimensionality of the interface layers modify the environment of the ions which in turn may influence the mechanism and strength of the correlations. Moreover, space charge effects at the interfaces may give raise to carrier concentration and mobility being substantially modified over the Debye screening length. In addition, epitaxial strain may be an important parameter in designing a high mobility landscape at the interface. Interface effects in epitaxial ionic conducting heterostructures appear as a promising pathway towards novel artificial electrolytes for cooler fuel cells although further work is warranted.[101] Combined experimental and theoretical efforts will be necessary for the understanding of the ultimate origin of the enhanced conductivity interface states. In particular, the predictive power of first principles tools may be determinant in the design of optimized interfaces for application in practical fuel cell devices.

Acknowledgements

Work at UCM and UPM supported by Spanish Ministry for Science and Innovation grants MAT2007 62162, and MAT2008 06517. Research at ORNL sponsored by the Division of Materials Sciences and Engineering of the US Department of Energy. Research at CINVESTAV has been supported by Mexican Conacyt (Grant SEP-2003-C02-44075).

Keywords: fuel cells · interfaces · ionics · solid electrolytes · superlattices

[1] W. R. Grove, *Phil. Mag. Ser. 3*, **1839**, *314*, 127.
[2] G. W. Crabtree, M. S. Dresselhaus, *MRS Bull.* **2008**, *33*, 421.
[3] N. P. Brandon, S. Skinner, B. C. H. Steele, *Annu. Rev. Mater. Res.* **2003**, *33*, 183.
[4] Z. Shao, S. M. Haile, *Nature* **2004**, *431*, 170.
[5] Y.-H. Huang, R. I. Das, Z.-L. Xing, J. B. Goodenough, *Science* **2006**, *312*, 254.
[6] S. Tao, J. T. S. Irvine, *Nat. Mater.* **2003**, *2*, 320–323.
[7] B. A. Boukamp, *Nat. Mater.* **2003**, *2*, 294.
[8] G. Kim, *Appl. Phys. Lett.* **2006**, *88*, 024103.
[9] B. C. H. Steele, A. Heinzel, *Nature* **2001**, *414*, 345.
[10] A. V. Chadwick, *Nature* **2000**, *408*, 925.
[11] T. H. Etsell, S. N. Flengas, *Chem. Rev.* **1970**, *70*, 339.
[12] A. P. Ramirez, A. Hayashi, R. J. Cava, R. Siddharthan, B. S. Shastry, *Nature* **1999**, *399*, 333.
[13] J. Snyder, J. S. Slusky, R. J. Cava, P. Schiffer, *Nature* **2001**, *413*, 48.
[14] W. J. Weber, R. C. Ewing, *Science* **2000**, *289*, 2051.
[15] P. K. Moon, H. L. Tuller in *Solid State Ionics* (Eds.: G. Nazri, R. A. Huggins, D. F. Shriver), *Mater. Res. Soc. Proc.* **1989**, 135, 149.
[16] J. Chen, J. Lian, L. M. Wang, R. C. Ewing, R. G. Wang, W. Pan, *Phys. Rev. Lett.* **2002**, *88*, 105901.
[17] B. J. Wuensch, K. W. Eberman, C. Heremans, E. M. Ku, P. Onnerud, E. M. E. Yeo, S. M. Haile, J. K. Stalick, J. D. Jorgensen, *Solid State Ionics* **2000**, *129*, 111.
[18] J. Maier, *Solid State Ionics* **2004**, *175*, 7.
[19] J. Maier, *Prog. Solid State Chem.* **1995**, *23*, 171–263.
[20] H. L. Tuller, *Solid State Ionics* **2000**, *131*, 143–157.
[21] L. Schlapbach, A. Zuttel, *Nature* **2001**, *414*, 353.
[22] A. C. Dillon, *Nature* **1997**, *386*, 377.
[23] A. S. Aricò, P. Bruce, B. Scrosati, J.-M. Tarascon, W. van Schalkwijk, *Nat. Mater.* **2005**, *4*, 366.
[24] J. Maier, *Nat. Mater.* **2005**, *4*, 805.
[25] J. Maier, *J. Electrochem. Soc.* **1987**, *134*, 1524.
[26] H. L. Tuller, *Solid State Ionics* **2000**, *131*, 143.
[27] J. Maier, *Solid State Ionics* **2002**, *154*, 291;J. Maier, *Solid State Ionics* **2003**, *157*, 327.
[28] K. L. Kliewer, J. S. Koehler, *Phys. Rev.* **1965**, *140*, A1226.
[29] E. B. Lavik, Y. M. Chiang, I. Kosacki, H. L Tuller, J. Y. Ying, *J. Electroceram.* **1997**, *1*, 7.
[30] I. Kosacki, T. Suzuki, V. Petrovsky, H. U. Anderson, *Solid State Ionics* **2000**, *136*, 1225.
[31] C. Peters, A. Weber, E. Ivers-Tiffee, H. Störmer, D. Gerthsen, M. Bockmeyer, R. Krüger, *Fall Materials Research Society (MRS) Meeting* **2006**, Boston, MA, 712.
[32] P. Mondal, H. Hahn, *Ber. Bunsen-Ges.* **1997**, *101*, 1765.
[33] S. Jiang, *J. Mater. Res.* **1997**, *12*, 2374.
[34] G. Knöner, K. Reinemann, R. Roewer, U. Soedervall, H.-E. Schaefer, *Proc. Natl. Acad. Sci. USA* **2003**, *100*, 3870.
[35] R. A. De Souza, M. J. Pietrovski, U. Anselmi-Tamburini, S. Kim, Z. A. Munir, M. Martín, *Phys. Chem. Chem. Phys.* **2008**, *10*, 2067.
[36] S. J. Litzelman, J. L. Hertz, W. Jung, H. Tuller, *Fuel Cells* **2008**, *8*, 294.
[37] B. C. H. Steele, *Eur. Fuel Cell News* **2000**, *7*, 16.
[38] K. W. Lux, K. J. Rodriguez, *Nano Lett.* **2006**, *6*, 288–295.
[39] V. R. Stamenkovic, B. Fowler, B. S. Mun, G. Wang, P. N. Ross, C. A. Lucas, N. M. Markovic, *Science* **2007**, *315*, 493.

 © 2009 Wiley-VCH Verlag GmbH & Co. KGaA, Weinheim

[40] J. Greeley, M. Mavrikakis, *Nat. Mater.* **2004**, *3*, 810.
[41] U. Sahaym, U. G. Norton, *J. Mater. Sci.* **2008**, *43*, 5395.
[42] L. Esaki, R. Tsu, *IBM J. Res. Dev.* **1970**, *14*, 61.
[43] I. K. Schuller, *Phys. Rev. Lett.* **1980**, *44*, 1597.
[44] M. N. Baibich, J. M. Broto, A. Fert, F. Nguyen Van Dau, F. Petroff, P. Eitenne, G. Creuzet, A. Friederich, J. Chazelas, *Phys. Rev. Lett.* **1988**, *61*, 2472.
[45] N. Sata, K. Eberman, K. Eberl, J. Maier, *Nature* **2000**, *408*, 946.
[46] I. Kosacki, B. Gorman, H. U. Anderson, *Ionic and Mixed Conductors, Vol. III* (Eds.: T. A. Ramanayanaran, W. L. Worrel, H. L. Tuller, A. C. Kandkar, M. Mogensen, W. Gopel), Electrochemical Society, Pennington, **1998**, p. 631.
[47] I. Kosacki, C. M. Rouleau, P. F. Becher, J. Bentley, D. H. Lowdness, *Solid State Ionics* **2005**, *176*, 1319.
[48] A. Karthikeyan, Ch. L. Chan, L. Ramanathan, *Appl. Phys. Lett.* **2006**, *89*, 183116.
[49] X. Guo, E. Vasco, S. Mi, K. Szot, E. Wachsman, R. Waser, *Acta Mater.* **2005**, *53*, 5161.
[50] P. Lacorre, F. Goutenoire, O. Bohnke, R. Retoux, Y. Laligant, *Nature* **2000**, *404*, 856.
[51] J. B. Goodenough, *Nature* **2000**, *404*, 821.
[52] K. J. Moreno, G. Mendoza-Suarez, A. F. Fuentes, J. Garcia-Barriocanal, C. Leon, J. Santamaria, *Phys. Rev. B* **2005**, *71*, 132301.
[53] M. Castro, A. Rivera, J. Garcia-Barriocanal, F. Dominguez-Adame, A. G. Belous, J. Santamaria, C. Leon, *Europhys. Lett.* **2005**, *69*, 770.
[54] C. P. Herrero, A. Varez, A. Rivera, J. Santamaria, C. Leon, O. V'yunov, A. G. Belous, J. Sanz, *J. Phys. Chem. B* **2005**, *109*, 3262.
[55] K. J. Moreno, A. F. Fuentes, M. Maczka, J. Hanuza, U. Amador, J. Santamaria, C. Leon, *Phys. Rev. B* **2007**, *75*, 184303.
[56] J. A. Díaz-Guillén, M. R. Díaz-Guillen, J. M. Almanza, A. F. Fuentes, J. Santamaria, C. Leon, *J. Phys. Condens. Matter* **2007**, *19*, 356212.
[57] M. R. Diaz-Guillén, K. J. Moreno, J. A. Diaz-Guillen, A. F. Fuentes, K. L. Ngai, J. Garcia-Barriocanal, J. Santamaria, C. Leon, *Phys. Rev. B* **2008**, *78*, 104304.
[58] J. Garcia-Barriocanal, A. Rivera-Calzada, M. Varela, Z. Sefrioui, E. Iborra, C. Leon, S. J. Pennycook, J. Santamaria, *Science* **2008**, *321*, 676.
[59] P. K. Moon, H. L. Tuller, *Solid State Ionics* **1988**, *28–30*, 470–474.
[60] M. Pirzada, R. W. Grimes, L. Minervini, J. F. Maguire, K. E. Sickafus, *Solid State Ionics* **2001**, *140*, 201–208.
[61] K. L. Ngai, C. Leon, *Phys. Rev. B* **1999**, *60*, 9396–9405.
[62] A. K. Jonscher, *Dielectric Relaxation in Solids*, Chelsea Dielectric Press, London, **1983**.
[63] P. B. Macedo, C. T. Moynihan, R. Bose, *Phys. Chem. Glasses* **1972**, *13*, 171.
[64] R. Kohlrausch, *Poggendorff's Ann. Phys.* **1847**, *72*, 353.
[65] K. Funke, R. D. Banhatti, *J. Non-Cryst. Solids* **2007**, *353*, 3845.
[66] K. L. Ngai, K. Y. Tsang, *Phys. Rev. E* **1999**, *60*, 4511.
[67] K. L. Ngai, C. Leon, *Phys. Rev. B* **2002**, *66*, 064308.
[68] K. L. Ngai, C. Leon, *J. Non-Cryst. Solids* **2003**, *315*, 124.
[69] A. F. Fuentes, K. Boulahya, M. Maczka, J. Hanuza, U. Amador, *Solid State Sci.* **2005**, *7*, 343.
[70] S. Azad, O. A. Marina, C. M. Wang, L. Saraf, V. Shutthanandan, D. E. McCready, A. El-Azab, J. E. Jaffe, M. H. Englehard, C. H. F. Peden, S. Thevuthasan, *Appl. Phys. Lett.* **2005**, *86*, 131906.
[71] C. M. Wang, M. H. Englehard, S. Azad, L. Saraf, O. A. Marina, D. E. McCready, V. Shutthanandan, Z. Q. Yu, S. Thevuthasan, M. Watanabe, D. B. Williams, *Solid State Ionics* **2006**, *177*, 1299.
[72] A. Peters, C. Korte, D. Hesse, N. Zakharov, J. Janek, *Solid State Ionics* **2007**, *178*, 67.
[73] C. Korte, A. Peters, J. Janek, D. Hesse, N. Zakharov, *Phys. Chem. Chem. Phys.* **2008**, *10*, 4623.
[74] A. Ohtomo, D. A. Muller, J. L. Grazul, H. Hwang, *Nature* **2002**, *419*, 378.
[75] A. Ohtomo, H. Hwang, *Nature* **2004**, *427*, 423.
[76] A. Brinkman, M. Huijben, M. van Zalk, J. Huijben, U. Zeitler, J. C. Maan, W. G. van der Wiel, G. Rijnders, D. H. A. Blank, H. Hilgenkamp, *Nat. Mater.* **2007**, *6*, 493.
[77] N. Reyren, S. Thiel, A. D. Caviglia, L. Fitting Kourkoutis, G. Hammerl, C. Richter, C. W. Schneider, T. Kopp, A.-S. Rüetschi, D. Jaccard, M. Gabay, D. A. Muller, J.-M. Triscone, J. Mannhart, *Science* **2007**, *317*, 1196.
[78] S. Thiel, G. Hammerl, A. Schmehl, C. W. Schneider, J. Mannhart, *Science* **2006**, *313*, 1942.
[79] S. Okamoto, A. Millis, *Nature* **2004**, *428*, 630.
[80] M. Varela, Z. Sefrioui, D. Arias, M. A. Navacerrada, M. Lucia, M. A. Lopez de La Torre, C. Leon, G. Loos, F. Sanchez-Quesada, J. Santamaria, *Phys. Rev. Lett.* **1999**, *83*, 3936.
[81] M. Varela, W. Grogger, D. Arias, Z. Sefrioui, C. Leon, C. Ballesteros, K. Krishnan, J. Santamaria, *Phys. Rev. Lett.* **2001**, *86*, 5156.
[82] Z. Sefrioui, D Arias, J. E. Villegas, M. Varela, V. Peña, P. Prieto, C. Leon, J. L. Martinez, J. Santamaria, *Phys. Rev. B* **2003**, *67*, 214511.
[83] V. Peña, Z. Sefrioui, M. Varela, D Arias, C. Leon, J. L. Martinez, S. J. Pennycook, J. Santamaria, *Phys. Rev. B* **2004**, *69*, 224502.
[84] Z. Sefrioui, V. Cros, A. Barthélémy, V. Peña, C. Leon, J. Santamaria, M. Varela, S. J. Pennycook, *Appl. Phys. Lett.* **2006**, *88*, 022512.
[85] C. León, M. L. Lucia, J. Santamaria, *Phys. Rev. B* **1997**, *55*, 882.
[86] A. Rivera, J. Santamaria, C. Leon, *Appl. Phys. Lett.* **2001**, *78*, 610.
[87] J. Wong, C. A. Angell, *Glass Structure by Spectroscopy*, Marcel Dekker, New York, **1976**.
[88] W. K. Lee, J. F. Liu, A. S. Nowick, *Phys. Rev. Lett.* **1991**, *67*, 1559.
[89] X. Lu, H. Jain, *J. Phys. Chem. Solids* **1994**, *55*, 1433.
[90] D. L. Sidebottom, P. F. Green, R. K. Brow, *Phys. Rev. Lett.* **1995**, *74*, 5068.
[91] H. Jain, X. Lu, *J. Non-Cryst. Solids* **1996**, *196*, 285.
[92] C. León, A. Rivera, A. Varez, J. Sanz. , J. Santamaria, K. L. Ngai, *Phys. Rev. Lett.* **2001**, *86*, 1279.
[93] A. Rivera, C. Leon, C. P. E. Varsamis, G. D. Chryssikos, K. L. Ngai, C. M. Roland, L. J. Buckley, *Phys. Rev. Lett.* **2002**, *88*, 125902.
[94] A. Rivera, C. Leon, J. Sanz, J. Santamaria, C. T. Moynihan, K. L. Ngai, *Phys. Rev. B* **2002**, *65*, 224302.
[95] C. León, A. Rivera, J. Santamaria, C. T. Moynihan, K. L. Ngai, *Phys. Rev. Lett.* **2002**, *89*, 079601.
[96] J. E. Bauerle, J. Hrizo, *J. Phys. Chem. Solids* **1969**, *30*, 565.
[97] J. D. Solier, I. Cachadiña, A. Dominguez-Rodriguez, *Phys. Rev. B* **1993**, *48*, 3704.
[98] K. L. Ngai, *J. Non-Cryst. Solids* **1996**, *203*, 232.
[99] R. J. Cava, E. A. Rietman, *Phys. Rev. B* **1984**, *30*, 6896.
[100] J. Fleig, H. L. Tuller, J. Maier, *Solid State Ionics* **2004**, *174*, 261.
[101] J. A. Kilner, *Nat. Mater.* **2008**, *7*, 838.

Received: October 17, 2008
Revised: February 23, 2009
Published online on March 27, 2009

 © 2009 Wiley-VCH Verlag GmbH & Co. KGaA, Weinheim